RESEARCH ARTICLE | SEPTEMBER 16 2022

Physical origin of vortex stretching and twisting: Viscous or inertial forces

L. M. Lin (林黎明) ✉ ; Y. X. Wu (吴应湘)

Physics of Fluids 34, 093108 (2022)
https://doi.org/10.1063/5.0108594

Physics of Fluids ARTICLE scitation.org/journal/phf

Physical origin of vortex stretching and twisting: Viscous or inertial forces

Cite as: Phys. Fluids **34**, 093108 (2022); doi: 10.1063/5.0108594
Submitted: 9 July 2022 · Accepted: 23 August 2022 ·
Published Online: 16 September 2022

L. M. Lin (林黎明),[1,a)] and Y. X. Wu (吴应湘)[1,2]

AFFILIATIONS

[1]Key Laboratory for Mechanics in Fluid Solid Coupling Systems, Institute of Mechanics, Chinese Academy of Sciences, Beijing 100190, China
[2]School of Engineering Sciences, University of Chinese Academy of Sciences, Beijing 100049, China

[a)]Author to whom correspondence should be addressed: llmbirthday@163.com

ABSTRACT

In this paper, the physical origin of vortex stretching and twisting is theoretically investigated. The effects of inertial and viscous forces are mainly considered and discussed. Two key conditions, i.e., solid walls and three-dimensional (3D) disturbances, are adopted in three typical cases. Among them, the first two cases are straight and curved vortex lines at the initial time without any kind of disturbance. The third case is a straight vortex line at the initial time with introduced 3D natural disturbances. Through experimental observations, numerical simulations, and theoretical analysis in these cases, the first two cases illustrate that the straight or curved vortex lines are still straight or curved at the next time, respectively, regardless of whether solid walls are introduced. However, the third case clearly shows that once natural disturbances are introduced, the straight vortex lines near and at solid walls at the initial time are stretched and twisted mainly by viscous forces, instead of inertial forces, typically demonstrated by the 3D wake transition of a straight circular cylinder and the transition of the laminar boundary layer at a flat plate. Accordingly, based on definitions of generation and enhancement in vortex stretching and twisting, it is confirmed that the viscous forces with two key conditions are the generation mechanism, while the inertial forces alone are the enhancement mechanism.

I. INTRODUCTION

A vortex is a basic kind and, in particular, an existing form of fluid motion originating from rotating fluid elements. There are so many kinds of vortices found as organized structures. In the first example, the typical forms in a bluff body's wake are the well-known Kármán vortex street alternately shed from a circular cylinder, two three-dimensional (3D) wake instability modes, i.e., modes A and B, and the large-scale vortex dislocations.[1–5] In the second example, the common form in the boundary layer is the hairpin(-like) vortex.[6,7] In the last example, helical vortex structures appear in many natural phenomena and structures, typically in the form of Beltrami flows.[8–18] Once formed, various vortices occupy only a very small portion of a flow but play a key role in organizing the flow, such as the sinews and muscles of the fluid motion[19] and the sinews of turbulence.[20] The generation, motion, evolution, instability, decay of vortices, and so on are all the subject of vortex dynamics.[21]

In vortex dynamics, it is well known that inertial forces and viscous forces play different roles in the vorticity transport equation.[22] The inertial forces mainly lead to vorticity convective transport and stretching of vortex lines, which intensifies the vorticity. However, viscous forces mainly generate and diffuse vorticity due to the action of viscosity. In addition, although Coriolis forces and shock fronts (namely, drastic pressure gradient) when hydraulics jump takes place can increase the vorticity, they are beyond the scope of the present paper and are not considered here.

Above all, it is necessary to introduce these different mechanisms of inertial and viscous forces into the vorticity equation. The Newtonian fluid used here is incompressible with constant density ρ and kinematic viscosity ν. The body forces are conservative, which, therefore, can be simplified as a part of the pressure. There is no heat transfer in the whole flow field. We, thus, begin with the dimensionless mass continuity and momentum equations written in an inertial frame of reference (x, y, and z) (under the proper initial and boundary conditions)

$$\nabla \cdot \boldsymbol{u} = 0, \tag{1}$$

$$\frac{\partial \boldsymbol{u}}{\partial t} + (\boldsymbol{u} \cdot \nabla)\boldsymbol{u} = \frac{\mathrm{D}\boldsymbol{u}}{\mathrm{D}t} = -\nabla p + \frac{1}{Re}\nabla^2 \boldsymbol{u}, \tag{2}$$

where $\boldsymbol{u}$ is the velocity vector with three components, i.e., u, v, and w along its own coordinates; t is the time; ∇ is the gradient operator defined by $\nabla = \frac{\partial}{\partial x}\boldsymbol{i} + \frac{\partial}{\partial y}\boldsymbol{j} + \frac{\partial}{\partial z}\boldsymbol{k}$, where $\boldsymbol{i}$, $\boldsymbol{j}$, and $\boldsymbol{k}$ are unit vectors defined as $\boldsymbol{i} = (1, 0, 0)$, $\boldsymbol{j} = (0, 1, 0)$, and $\boldsymbol{k} = (0, 0, 1)$, respectively, giving $\nabla^2 = \frac{\partial^2}{\partial x^2} + \frac{\partial^2}{\partial y^2} + \frac{\partial^2}{\partial z^2}$; $\mathrm{D}/\mathrm{D}t$ is the Lagrangian derivative; p is the pressure; and Re is the Reynolds number defined as $U_\infty L/\nu$, where U_∞ is the characteristic velocity and L is the characteristic length. Velocities are scaled by U_∞ and lengths by L.

Then, based on the definition of the vorticity vector, i.e., $\boldsymbol{\omega} = \nabla \times \boldsymbol{u}$, taking the curl of the above momentum equation, Eq. (2), gives

$$\frac{\partial \boldsymbol{\omega}}{\partial t} + (\boldsymbol{u} \cdot \nabla)\boldsymbol{\omega} = \frac{\mathrm{D}\boldsymbol{\omega}}{\mathrm{D}t} = (\boldsymbol{\omega} \cdot \nabla)\boldsymbol{u} + \frac{1}{Re}\nabla^2\boldsymbol{\omega}. \tag{3}$$

This is the general form of the nondimensional vorticity equation. As stated in previous literature,[22] the second term on the left side, $(\boldsymbol{u} \cdot \nabla)\boldsymbol{\omega}$, is the convective transport of vorticity. The second from the last term, $(\boldsymbol{\omega} \cdot \nabla)\boldsymbol{u}$, represents the stretching of vortex lines. The viscous diffusion of vorticity is represented by the last term, $\nabla^2\boldsymbol{\omega}/Re$.

Subsequently, as shown in Fig. 1, the nonlinear stretching term, $(\boldsymbol{\omega} \cdot \nabla)\boldsymbol{u}$, can be rewritten as follows:

$$\begin{aligned}(\boldsymbol{\omega} \cdot \nabla)\boldsymbol{u} &= |\boldsymbol{\omega}| \lim_{\mathrm{P_2P_1}\to 0} \frac{\delta \boldsymbol{u}}{\mathrm{P_2P_1}} = |\boldsymbol{\omega}| \lim_{\delta l \to 0} \frac{\delta \boldsymbol{u}}{\delta l} \\ &= |\omega| \lim_{\delta l \to 0} \frac{\delta \boldsymbol{u}_\parallel}{\delta l} + |\boldsymbol{\omega}| \lim_{\delta l \to 0} \frac{\delta \boldsymbol{u}_\perp}{\delta l},\end{aligned} \tag{4}$$

where $\mathrm{P_1}$ and $\mathrm{P_2}$ are two adjacent points on the vortex line with a distance of δl at the same moments and where $\delta \boldsymbol{u}$ is the relative velocity at position $\mathrm{P_2}$ relative to the velocity at position $\mathrm{P_1}$. Consequently, this local relative velocity vector $\delta \boldsymbol{u}$ can be divided into a component $\delta \boldsymbol{u}_\parallel$ parallel to the vortex line and a component $\delta \boldsymbol{u}_\perp$ perpendicular to the vortex line. Therefore, in Eq. (4), the term $|\boldsymbol{\omega}| \lim_{\delta l \to 0} \frac{\delta \boldsymbol{u}_\parallel}{\delta l}$ represents the stretching of the vortex line, while the term $|\boldsymbol{\omega}| \lim_{\delta l \to 0} \frac{\delta \boldsymbol{u}_\perp}{\delta l}$ represents the twisting of the vortex line.

Recently, after introducing two key conditions, it was theoretically verified that viscous forces have the indirect physical mechanism of vortex stretching and twisting.[23] The first condition is the nonslip boundary condition at solid walls or the existence of such solid walls with a large velocity gradient associated with the fluid viscosity. The second condition is the induction or generation of disturbed vorticity, which can be attributed to 3D geometric or artificial disturbances or perturbed velocity due to 3D instability or turbulence. In the immediate neighborhood of solid walls, where the viscous forces are far greater than the inertial forces, the local spanwise vortex in shear flows at walls can be stretched or compressed and twisted by the viscous forces.

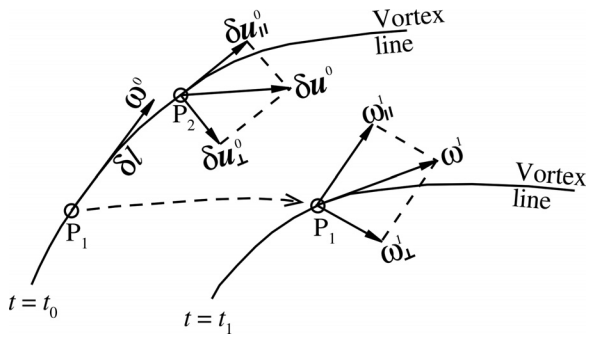

FIG. 1. Schematic diagram of the spatiotemporal evolution of curved vortex lines (denoted by solid lines) at the initial time t_0 and the next time t_1. In the meantime, the fluid particle at the position $\mathrm{P_1}$ and at the initial time t_0 moves to a new position also marked by the same position $\mathrm{P_1}$ at the next time t_1, which is denoted by the dashed line with arrow.

Consequently, a more profound physical problem is naturally proposed. Both inertial forces and viscous forces can produce the effect of vortex stretching and twisting, regardless of the direct or indirect effect. From the perspective of the physical mechanism of vortex stretching and twisting itself, it would be very interesting to determine the physical source or origin: inertial or viscous forces. In other words, two opposite processes should be clarified as follows. The viscous forces initially produce vortex stretching and twisting, and then the inertial forces reinforce such a physical effect. On the contrary, the inertial forces initially lead to vortex stretching and twisting, and the viscous forces, thus, intensify this physical mechanism.

To the best of our knowledge, there is no literature addressing this physical origin of vortex stretching and twisting owing to inertial or viscous forces. Therefore, in this paper, the main aim is to explore this physical origin problem in vortex stretching and twisting. The central issue is the condition in the transition from the straight vortex line at the initial time to the curved vortex line at the next time.

II. ANALYTICAL MODEL

As shown in Fig. 1, the spatiotemporal evolution of curved vortex lines at two consecutive times, t_0 and t_1, is illustrated. At the initial time t_0, there are the local vorticity vector $\boldsymbol{\omega}^0$ at position $\mathrm{P_1}$ and the decomposition of the local relative velocity vector $\delta \boldsymbol{u}^0$ along both parallel and perpendicular directions at position $\mathrm{P_2}$. At the next time t_1, the fluid element at the original position $\mathrm{P_1}$ and at the initial time t_0 moves to a new position, also marked by the same position $\mathrm{P_1}$, because the fluid element is the same. Moreover, there is a new vorticity vector $\boldsymbol{\omega}^1$ and its two orthogonal vector components $\boldsymbol{\omega}^1_\parallel$ and $\boldsymbol{\omega}^1_\perp$.

Then, for analytical convenience, the original vortex equation (3) can be modified. First, taking into account the decomposition of the local relative velocity vector $\delta \boldsymbol{u}^0$, vectors in the other two terms in Eq. (3) can be rewritten as follows:

$$\frac{\mathrm{D}\boldsymbol{\omega}}{\mathrm{D}t} = \left(\frac{\mathrm{D}\boldsymbol{\omega}}{\mathrm{D}t}\right)_\parallel + \left(\frac{\mathrm{D}\boldsymbol{\omega}}{\mathrm{D}t}\right)_\perp, \tag{5a}$$

$$\frac{1}{Re}\nabla^2\boldsymbol{\omega} = \frac{1}{Re}(\nabla^2\boldsymbol{\omega})_\parallel + \frac{1}{Re}(\nabla^2\boldsymbol{\omega})_\perp. \tag{5b}$$

Resultantly, the original vortex equation (3) can then be divided into the following two parts:

$$\left(\frac{\mathrm{D}\boldsymbol{\omega}}{\mathrm{D}t}\right)_\parallel = |\boldsymbol{\omega}| \lim_{\delta l \to 0} \frac{\delta \boldsymbol{u}_\parallel}{\delta l} + \frac{1}{Re}(\nabla^2\boldsymbol{\omega})_\parallel, \tag{6a}$$

$$\left(\frac{\mathrm{D}\boldsymbol{\omega}}{\mathrm{D}t}\right)_\perp = |\boldsymbol{\omega}| \lim_{\delta l \to 0} \frac{\delta \boldsymbol{u}_\perp}{\delta l} + \frac{1}{Re}(\nabla^2\boldsymbol{\omega})_\perp. \tag{6b}$$

Moreover, some assumptions are given as follows:

(1) The first-order approximation is adopted when the time step is small enough, i.e., $\delta t = t_1 - t_0 \to 0$, $\frac{\mathrm{D}\boldsymbol{\omega}}{\mathrm{D}t} \simeq \frac{\boldsymbol{\omega}^1 - \boldsymbol{\omega}^0}{\delta t}$ is assumed

accordingly. Furthermore, the relationship between $\boldsymbol{\omega}^1$ and $\boldsymbol{\omega}^0$ can be prescribed by $\boldsymbol{\omega}^1_{\parallel} \parallel \boldsymbol{\omega}^0$ and $\boldsymbol{\omega}^1_{\perp} \perp \boldsymbol{\omega}^0$, as shown in Fig. 1.

(2) When the distance between P_2 and P_1 is small enough, i.e., $\delta l \to 0$, two relationships are assumed, i.e., $\delta \boldsymbol{u}^0_{\parallel} \parallel \boldsymbol{\omega}^0$ and $\delta \boldsymbol{u}^0_{\perp} \perp \boldsymbol{\omega}^0$.

(3) The vorticity equation (3) is assumed to be explicitly expressed, then two terms on the right side are written at initial time t_0, i.e., $[(\boldsymbol{\omega}\cdot\nabla)\boldsymbol{u}]^0 = |\boldsymbol{\omega}^0| \lim_{\delta l\to 0} \frac{\delta \boldsymbol{u}^0}{\delta l}$, and $\frac{1}{Re}(\nabla^2\boldsymbol{\omega})^0 = \nabla^2\boldsymbol{\omega}^0/Re$.

Consequently, Eq. (6) can be rewritten as follows:

$$\frac{\boldsymbol{\omega}^1_{\parallel} - \boldsymbol{\omega}^0}{\delta t} = |\boldsymbol{\omega}^0| \lim_{\delta l\to 0} \frac{\delta \boldsymbol{u}^0_{\parallel}}{\delta l} + \frac{1}{Re}(\nabla^2\boldsymbol{\omega}^0)_{\parallel}, \tag{7a}$$

$$\frac{\boldsymbol{\omega}^1_{\perp}}{\delta t} = |\boldsymbol{\omega}^0| \lim_{\delta l\to 0} \frac{\delta \boldsymbol{u}^0_{\perp}}{\delta l} + \frac{1}{Re}(\nabla^2\boldsymbol{\omega}^0)_{\perp}. \tag{7b}$$

More specifically, the analytical model for investigating the physical origin of vortex stretching and twisting is presented as follows:

$$\boldsymbol{\omega}^1_{\parallel} = \boldsymbol{\omega}^0 + \delta t|\boldsymbol{\omega}^0| \lim_{\delta l\to 0} \frac{\delta \boldsymbol{u}^0_{\parallel}}{\delta l} + \frac{\delta t}{Re}(\nabla^2\boldsymbol{\omega}^0)_{\parallel} \tag{8a}$$

$$\boldsymbol{\omega}^1_{\perp} = \delta t|\boldsymbol{\omega}^0| \lim_{\delta l\to 0} \frac{\delta \boldsymbol{u}^0_{\perp}}{\delta l} + \frac{\delta t}{Re}(\nabla^2\boldsymbol{\omega}^0)_{\perp}. \tag{8b}$$

This analytical model clearly indicates several following situations:

(A1) The generation and enhancement of $\boldsymbol{\omega}^1_{\parallel}$ is mainly determined by the initial vorticity $\boldsymbol{\omega}^0$, the vortex stretching term $|\boldsymbol{\omega}^0| \lim_{\delta l\to 0} \frac{\delta \boldsymbol{u}^0_{\parallel}}{\delta l}$ and the viscous diffusion term $(\nabla^2\boldsymbol{\omega}^0)_{\parallel}$.

(A2) The nonzero vortex stretching or viscous diffusion term results in $\boldsymbol{\omega}^1_{\parallel}$ being different from $\boldsymbol{\omega}^0$ along its own rotational direction.

(A3) Otherwise, both the vortex stretching term and the viscous diffusion term disappear, and $\boldsymbol{\omega}^1_{\parallel}$ is exactly the same as $\boldsymbol{\omega}^0$.

(B1) However, the generation and enhancement of $\boldsymbol{\omega}^1_{\perp}$ is dependent only on the vortex twisting term $|\boldsymbol{\omega}^0| \lim_{\delta l\to 0} \frac{\delta \boldsymbol{u}^0_{\perp}}{\delta l}$ and the viscous diffusion term $(\nabla^2\boldsymbol{\omega}^0)_{\perp}$.

(B2) Once $\boldsymbol{\omega}^1_{\perp} = 0$, it signifies that the physical effect of vortex twisting disappears at the next time. Therefore, in the following analysis, the generation and enhancement of $\boldsymbol{\omega}^1_{\perp}$ is used to determine whether the vortex line is straight or curved at the next time.

Based on these descriptions, two definitions of the generation and enhancement of vorticity are clarified as follows. (1) The term "generation" indicates the value of vorticity from zero to nonzero, which is the qualitative variation owing to the appearance of nonzero vorticity. (2) The term "enhancement" means that the value of vorticity quantitatively varies, such as from 1 to 10.

Similarly, for vortex stretching and twisting, these two concepts are briefly described. The generation mechanism shows that the vorticity initially begins to change along its rotation axis and develops from a straight vortex into a curved vortex as time passes. For example, as shown in Fig. 1, at the initial time t_0, there is $(\boldsymbol{\omega}^0)_{P1} = (\boldsymbol{\omega}^0)_{P2}$ first in the same straight vortex line with $(\boldsymbol{\omega}^0\cdot\nabla)\boldsymbol{u}^0 = 0$. And then at the next time t_1, we have $(\boldsymbol{\omega}^1_{\parallel})_{P1} \neq (\boldsymbol{\omega}^0)_{P1}$ and $(\boldsymbol{\omega}^1_{\perp})_{P1} \neq 0$ with $(\boldsymbol{\omega}^1\cdot\nabla)\boldsymbol{u}^1 \neq 0$. However, the enhancement mechanism manifests an initially curved vortex still twisted at the next time. For example, also as shown in Fig. 1, at the initial time t_0, there is $(\boldsymbol{\omega}^0)_{P1} \neq (\boldsymbol{\omega}^0)_{P2}$ first in the same curved vortex line with $(\boldsymbol{\omega}^0\cdot\nabla)\boldsymbol{u}^0 \neq 0$. And then at the next time t_1, we have $(\boldsymbol{\omega}^1_{\parallel})_{P1} \neq (\boldsymbol{\omega}^0)_{P1}$ and $(\boldsymbol{\omega}^1_{\perp})_{P1} \neq 0$ with $(\boldsymbol{\omega}^1\cdot\nabla)\boldsymbol{u}^1 \neq 0$. Accordingly, the generation mechanism is the physical origin of vortex stretching and twisting, but the enhancement mechanism is just the sustaining of already generated vortex stretching and twisting. It should be noted in the above concepts and the following analysis that the nonzero vorticity at the initial time t_0 is still nonzero at the next time t_1 although this vorticity ultimately dissipates due to viscous diffusion.

III. RESULTS AND DISCUSSION

The key point in identifying the physical origin of vortex stretching and twisting is to determine certain conditions in the transition from the straight vortex into the curved vortex. On the basis of previous research,[23] two introduced conditions, i.e., solid walls and velocity or vorticity disturbances, are also used here. Different cases associated with these two conditions are presented. First, two cases without any kind of disturbance are studied and analyzed. In these two cases, one involves straight vortex lines at initial time t_0, while the other involves curved vortex lines at $t = t_0$. Then, the third case involves the initially straight vortex lines near the solid walls under 3D natural disturbances.

A. First case: Straight vortex lines at $t = t_0$ with no disturbance

1. Infinite flow domain without solid walls

As shown in Fig. 2(a), straight vortex lines in a vortex tube along the z-axis at $t = t_0$ are illustrated with the vortex center at position (x_0, y_0). The flow field is infinite without any solid wall. Such straight vortex tube can be generated by the Kelvin–Helmholtz instability in a strictly two-dimensional (2D) mixing layer, e.g., in the (x, y) plane, without any disturbance (or turbulence) in the z-axis.[22] The local velocity field around vortex lines is 2D, that is, $\boldsymbol{u}^0 = (u^0, v^0, w^0)$, where $u^0(x, y) \neq 0$, $v^0(x, y) \neq 0$ and $w^0 = 0$. The vorticity vector is obtained as follows: $\boldsymbol{\omega}^0 = (\omega^0_x, \omega^0_y, \omega^0_z)$, where $\omega^0_x = \omega^0_y = 0$ and $\omega^0_z = \frac{\partial v^0}{\partial x} - \frac{\partial u^0}{\partial y} \neq 0$. Here, the case with $\omega^0_z > 0$ is considered and discussed. The variation in ω^0_z along both the x- and y-axes is assumed to be maximal at position (x_0, y_0) but gradually decays away from the center due to the fluid viscosity, as shown in Fig. 2(b). Then, the vorticity vector at two successive times, t_0 and t_1, can be simplified in the present case as follows, $\boldsymbol{\omega}^0 = \omega^0_z\boldsymbol{k}$ and $\boldsymbol{\omega}^1 = \boldsymbol{\omega}^1_{\parallel} + \boldsymbol{\omega}^1_{\perp}$, in which $\boldsymbol{\omega}^1_{\parallel} = \omega^1_z\boldsymbol{k}$ and $\boldsymbol{\omega}^1_{\perp} = \omega^1_x\boldsymbol{i} + \omega^1_y\boldsymbol{j}$.

For $\boldsymbol{\omega}^1_{\parallel}$ in Eq. (8a), the stretching and diffusion terms can be solved. First, the stretching term is given by $|\boldsymbol{\omega}^0| \lim_{\delta l\to 0} \frac{\delta \boldsymbol{u}^0_{\parallel}}{\delta l} = \omega^0_z \frac{\partial w^0}{\partial z}\boldsymbol{k} \equiv 0$. This shows that the stretching effect disappears. Then, the diffusion term is expressed by $\frac{1}{Re}(\nabla^2\boldsymbol{\omega}^0)_{\parallel} = \frac{1}{Re}\nabla^2\omega^0_z\boldsymbol{k}$ with $\nabla^2\omega^0_z < 0$ near position (x_0, y_0) in the viscous fluid, or $\frac{1}{Re}(\nabla^2\boldsymbol{\omega}^0)_{\parallel} = 0$ in the inviscid fluid. This leads to $|\boldsymbol{\omega}^1_{\parallel}| = \omega^1_z \leq |\boldsymbol{\omega}^0| = \omega^0_z$.

For $\boldsymbol{\omega}^1_{\perp}$ in Eq. (8b), the twisting and diffusion terms are obtained. The twisting term is solved as $|\boldsymbol{\omega}^0| \lim_{\delta l\to 0} \frac{\delta \boldsymbol{u}^0_{\perp}}{\delta l} = \omega^0_z \frac{\partial u^0}{\partial z}\boldsymbol{i} + \omega^0_z \frac{\partial v^0}{\partial z}\boldsymbol{j} \equiv 0$. This result clearly verifies the disappearance of the

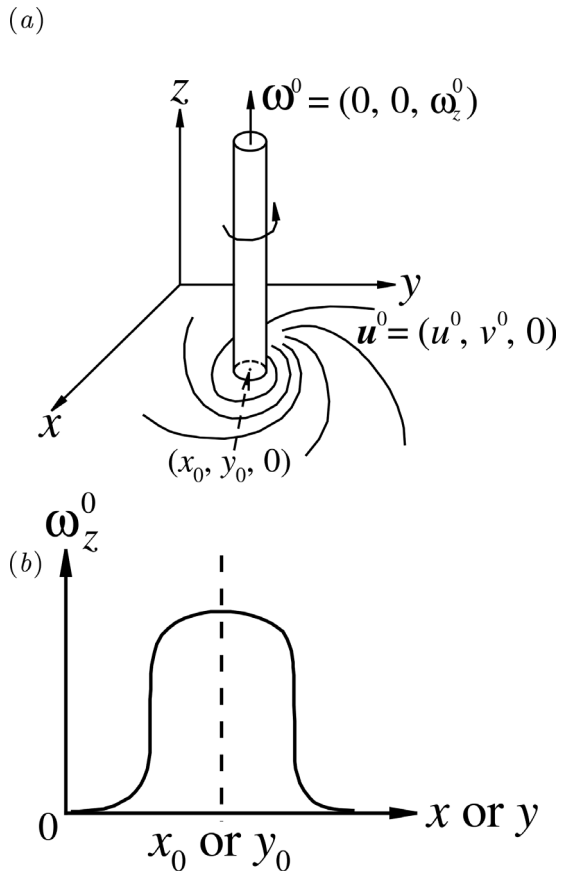

FIG. 2. Sketches of (a) a straight vortex tube with its rotational direction along the z-axis, i.e., $\boldsymbol{\omega}^0 = (0, 0, \omega_z^0)$, in the infinite flow region at the initial time t_0 and with the vortex center at position (x_0, y_0) and (b) its amplitude ω_z^0 varying along the x- or y-axis.

twisting effect. Moreover, in the diffusion term, $\frac{1}{Re}(\nabla^2\boldsymbol{\omega}^0)_\perp = \frac{1}{Re}\nabla^2\omega_x^0\boldsymbol{i} + \frac{1}{Re}\nabla^2\omega_y^0\boldsymbol{j} \equiv 0$, regardless of the viscous or inviscid fluid. This leads to $\boldsymbol{\omega}_\perp^1 \equiv 0$ or $\omega_x^1 \equiv 0$ and $\omega_y^1 \equiv 0$.

Therefore, it can be obtained that $|\boldsymbol{\omega}^1| = |\boldsymbol{\omega}_\parallel^1| = \omega_z^1 \le |\boldsymbol{\omega}^0| = \omega_z^0$, indicating that the vorticity $|\boldsymbol{\omega}|$ reduces only under the viscous dissipation effect or remains constant in the inviscid fluid.

These results clearly show that the straight vortex at the initial time undergoes straight formation at the next time without any stretching or twisting, but the vorticity decreases due to nonzero viscous diffusion and dissipation of the vorticity or remains constant indefinitely when the fluid is inviscid.

2. Finite flow domain near solid walls

When solid walls are introduced as the first key condition, as shown in Fig. 3, two typical flows are analyzed. The first is the flow past a bluff body, typically a straight cylinder with a circular cross section, at low Reynolds numbers before the 3D instability occurs. The second is the shear flow near solid walls, typically the laminar boundary layer at a flat plate at zero incidence.

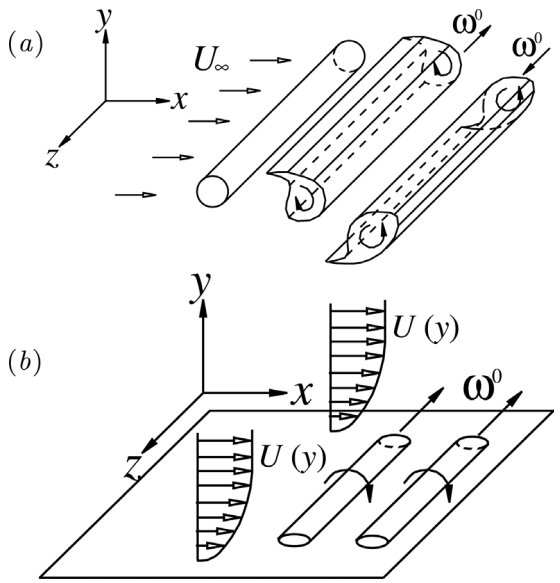

FIG. 3. Sketches of straight vortex tubes in (a) the near wake of 2D bluff body at low Reynolds numbers and (b) the laminar boundary layer at a flat plate without any disturbance.

In the wake flow of a circular cylinder, as reported in the previous works,[1,5] the near wake is 2D at $Re < 140$–145. When $Re < 50$, the shear flow is attached on cylinder surfaces, with a pair of symmetrical vortices on the rear surface. As the Reynolds number exceeds 50 and increases to $140 \sim 145$, the near wake can be described by alternately shedding Kármán vortices because of the onset of the wake instability as the manifestation of Hopf bifurcation, as shown in Fig. 3(a). These Kármán vortex streets can be demonstrated by isosurfaces or contours of spanwise vorticity. Among them, $\boldsymbol{\omega}^0 = -|\omega_z^0|\boldsymbol{k}$ holds in the clockwise primary vortex shedding from the upper side of the cylinder, while $\boldsymbol{\omega}^0 = +|\omega_z^0|\boldsymbol{k}$ holds in the anticlockwise spanwise vortex shedding from the lower side of the cylinder.

In the laminar boundary layer at a flat plate with zero incidence, as already presented in Ref. 24, the shear flow is stable and 2D before the appearance or introduction of disturbances, such as the instability of traveling, 2D Tollmien–Schlichting (T–S) waves or unsteady, laminar, and 3D waves due to secondary instabilities, as shown in Fig. 3(b). Here, because the nonuniform streamwise velocity $U(y)$ increases along the vertical distance y away from the plate at $y = 0$, then, $\boldsymbol{\omega}^0 = -|\omega_z^0|\boldsymbol{k}$ appears in the whole laminar boundary layer, and the vorticity $|\omega_z^0|$ gradually decreases with increasing y.

A similar analysis can also be carried out in both typical flows. Similar features in the distributions of velocity vector $\boldsymbol{u}^0 = (u^0, v^0, w^0)$ and vorticity vector $\boldsymbol{\omega}^0 = (\omega_x^0, \omega_y^0, \omega_z^0)$ are presented as follows: (1) $w^0 = \omega_x^0 = \omega_y^0 = 0$; (2) $u^0(x, y) \neq 0$ and $v^0(x, y) \neq 0$ in the near wake; or (3) $u^0(y) = U(y)$ and $v^0 = 0$ in the laminar boundary layer; (4) then, $\omega_z^0 \neq 0$. Therefore, similar conclusions, as stated in detail in the above subsection, can be made, particularly for the remaining disappearance of the twisting term and $\boldsymbol{\omega}_\perp^1$.

In summary, whether solid walls are introduced or not, under present circumstances (i.e., without any kind of disturbance), the

straight vortex line at $t = t_0$ is still straight at $t = t_1$ with the absence of any vortex stretching and twisting.

B. Second case: Curved vortex lines at $t = t_0$ with no disturbance

1. Infinite flow domain without solid walls

For the convenience of analysis, and without loss of generality, as shown in Fig. 4, some assumptions in the analysis of the curved vortex line at $t = t_0$ are presented as follows:

(1) The analyzed fluid element at position P_1 in Figs. 1 and 4 is located at the origin of the Cartesian coordinate system, i.e., $(x = 0, y = 0, \text{and } z = 0)$.
(2) The direction of vortex vector $\boldsymbol{\omega}^0$ at position P_1 is aligned to the $+z$-axis.
(3) The curved vortex line between two positions P_2 and P_1 is located in the (y, z) plane.

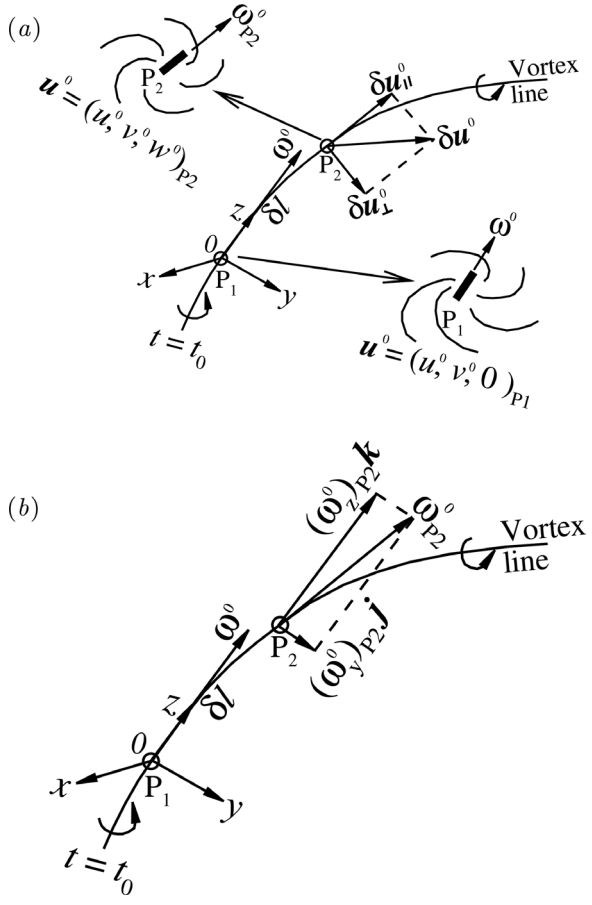

FIG. 4. Schematic diagrams of (a) a curved vortex line at the initial time t0 with the specific Cartesian coordinate system (x, y, and z) established at position P_1 and the local velocity distributions near positions P_1 and P_2, where two thick and short line segments indicate the local vortex lines at positions P_1 and P_2, respectively and (b) the decomposition of vorticity vector at position P_2.

Similarly, this curved vortex line can be generated in the 3D mixing transition, typically in the appearance of helical pairing.[22,25] Some experiments indicate the presence of longitudinal vortices stretched into "hairpins" between the Kelvin–Helmholtz spiral vortices.

Then, the velocity and vorticity fields at $t = t_0$ around the curved vortex line are typically 3D. As shown in Fig. 4, the velocity vector near position P_1 is almost 2D, i.e., $(\boldsymbol{u}^0)_{P1} = (u^0, v^0, 0)_{P1}$, associated with the local vorticity vectors $\boldsymbol{\omega}^0 = \omega_z^0 \boldsymbol{k}$ $(\omega_z^0 > 0)$ and $\omega_x^0 = \omega_y^0 = 0$ at position P_1, based on the above assumptions. However, near position P_2, the curved vortex line between positions P_2 and P_1 leads to the vorticity vector at position P_2, $\boldsymbol{\omega}_{P2}^0$, slightly skewed away from the direction of $\boldsymbol{\omega}^0$ at position P_1 in the (y, z) plane, as shown in Fig. 4. Correspondingly, at position P_2, ω_y^0 is nonzero, while ω_x^0 is still zero, then, $\boldsymbol{\omega}_{P2}^0 = (\omega_y^0)_{P2}\boldsymbol{j} + (\omega_z^0)_{P2}\boldsymbol{k}$. Consequently, the local velocity vector near position P_2 by Biot–Savart induction is certainly 3D because of the appearance of nonzero spanwise velocity, i.e., $(\boldsymbol{u}^0)_{P2} = (u^0, v^0, w^0)_{P2}$.

At the next time t_1, the relationships between $\boldsymbol{\omega}^0$ and $\boldsymbol{\omega}^1$ for the fluid element of P_1 are still valid: $\boldsymbol{\omega}^0 = \omega_z^0 \boldsymbol{k}$ and $\boldsymbol{\omega}^1 = \boldsymbol{\omega}_{\parallel}^1 + \boldsymbol{\omega}_{\perp}^1$, where $\boldsymbol{\omega}_{\parallel}^1 = \omega_z^1 \boldsymbol{k}$ and $\boldsymbol{\omega}_{\perp}^1 = \omega_x^1 \boldsymbol{i} + \omega_y^1 \boldsymbol{j}$.

For $\boldsymbol{\omega}_{\parallel}^1$ in Eq. (8a), the stretching and diffusion terms can be analyzed similarly as follows. First, the stretching term is given by $|\boldsymbol{\omega}^0| \lim_{\delta l \to 0} \frac{\delta \boldsymbol{u}_{\parallel}^0}{\delta l} = \omega_z^0 \lim_{\delta l \to 0} \frac{(w^0)_{P2}}{\delta l} \boldsymbol{k} = \omega_z^0 \frac{\partial w^0}{\partial z} \boldsymbol{k} \neq 0$. This shows that the stretching effect still exists. Then, the diffusion term is expressed by $\frac{1}{Re}(\nabla^2 \boldsymbol{\omega}^0)_{\parallel} = \frac{1}{Re} \nabla^2 \omega_z^0 \boldsymbol{k} \neq 0$ in the viscous fluid, or $\frac{1}{Re}(\nabla^2 \boldsymbol{\omega}^0)_{\parallel} = 0$ in the inviscid fluid. This leads to $|\boldsymbol{\omega}_{\parallel}^1| = \omega_z^1 \neq |\boldsymbol{\omega}^0| = \omega_z^0$.

For $\boldsymbol{\omega}_{\perp}^1$ in Eq. (8b), the twisting and diffusion terms are obtained as follows. The twisting term is given by $|\boldsymbol{\omega}^0| \lim_{\delta l \to 0} \frac{\delta \boldsymbol{u}_{\perp}^0}{\delta l} \simeq \omega_z^0 \frac{\partial u^0}{\partial z} \boldsymbol{i} + \omega_z^0 \frac{\partial v^0}{\partial z} \boldsymbol{j}$. If there is no twisting term, specific conditions, $\frac{\partial u^0}{\partial z} = 0$ and $\frac{\partial v^0}{\partial z} = 0$, should be satisfied at the same time. The definition of $\omega_z = \frac{\partial v}{\partial x} - \frac{\partial u}{\partial y}$ gives $\frac{\partial \omega_z^0}{\partial z} \equiv 0$. Moreover, $\omega_x^0 = 0$ in the present curved vortex line in the (y, z) plane gives $\frac{\partial \omega_x^0}{\partial x} = 0$. The relationship, $\nabla \cdot \boldsymbol{\omega} = 0$, thus, gives $\frac{\partial \omega_y^0}{\partial y} = 0$. The situation with $\frac{\partial \omega_y^0}{\partial y} = 0$ between positions P_2 and P_1 is inconsistent with the present curved vortex line, in which ω_y^0 at P_2 appears while ω_y^0 at P_1 disappears. Therefore, this paradox verifies that the twisting term always exists in the present case. In the diffusion term, $\frac{1}{Re}(\nabla^2 \boldsymbol{\omega}^0)_{\perp} = \frac{1}{Re} \nabla^2 \omega_y^0 \boldsymbol{j}$ appears in the viscous fluid or disappears in the inviscid fluid. Finally, this leads to $\boldsymbol{\omega}_{\perp}^1 \neq 0$.

These results clearly show that the curved vortex at the initial time keeps the curved formation at the next time with certain vortex stretching and twisting.

2. Finite flow domain near solid walls

Similarly, two typical flows, i.e., the wake flow of a bluff body and the boundary layer at a flat plate, are discussed here, as the first introduced key condition of solid walls. The term "no disturbance" in the present subsection means that once vortex lines are curved or twisted, no artificial or natural disturbance is introduced. Only the curved vortex lines at two adjacent times t_0 and t_1 are presented and discussed. Besides, as pointed out by Gresho,[26] improper initial and boundary conditions in numerical simulations will result in spurious solutions or

unreal flows, particularly in the wake of a bluff body.[4,5] To avoid the great influence of initial conditions on numerical results, the computational time is long enough until the wake flow is fully developed. In order to minimize the effect of boundary conditions (especially outflow boundary conditions) on simulations, the computational domain is large enough. These independence studies are already carried out and reported in the previous works.[4,5]

In the near wake of a circular cylinder, as the first example, the first 3D instability mode, i.e., pure mode A without the interference of vortex dislocations, is presented. As already reported in the previous works,[5] the second critical Reynolds number of approximately 195 denotes the transition from the initially generated pure mode A to the fully developed pure mode A. In the full development stage, as shown in Fig. 5 through direct numerical simulations (DNS), pure mode A can be described by alternately shedding primary vortices wavily twisted across the span.[1–4] At two typical times T_0 and T_1, as shown in Fig. 5(a), vortex lines in different shedding spanwise vortices are always twisted across the span, as shown in Figs. 5(c) and 5(d). On the other hand, as shown in Fig. 5(b), as an example, curved vortex A at present T_0 will become curved vortex B at the next T_0 after a whole shedding period. Moreover, the isosurface of vortex B with $\omega_z = 0.5$ is notably smaller than that of vortex A because of the viscous diffusion and dissipation. These results clearly demonstrate that in the near wake far away from the cylinder, inertial forces lead to curved vortices continuously stretching and twisting over time, while viscous forces mainly result in vorticity diffusion and dissipation.

In laminar and turbulent boundary layers at a flat plate, as the second example, there are several models for describing the 3D shape of eddies as typical coherent structures,[27] which is typically the predominant role of Townsend's attached eddies.[28] The most widespread model is probably the hairpin vortex paradigm, which advocates for attached loop-like vortices or hairpin vortices. The classic hairpin vortex paradigm was originally proposed by Theodorsen,[6] as shown in Fig. 6(a). Under the present circumstances, such a hairpin vortex is assumed to be simplified as a vortex line in the center of the hairpin vortex, as shown in Fig. 6(b). Moreover, the local coordinate system $(x_0, y_0,$ and $z_0)$ is established at the top of the head, as shown in Figs. 6(b) and 6(c). The local head and adjacent leg are assumed to be in the local (y_0, z_0) plane. Therefore, the analysis presented in the infinite

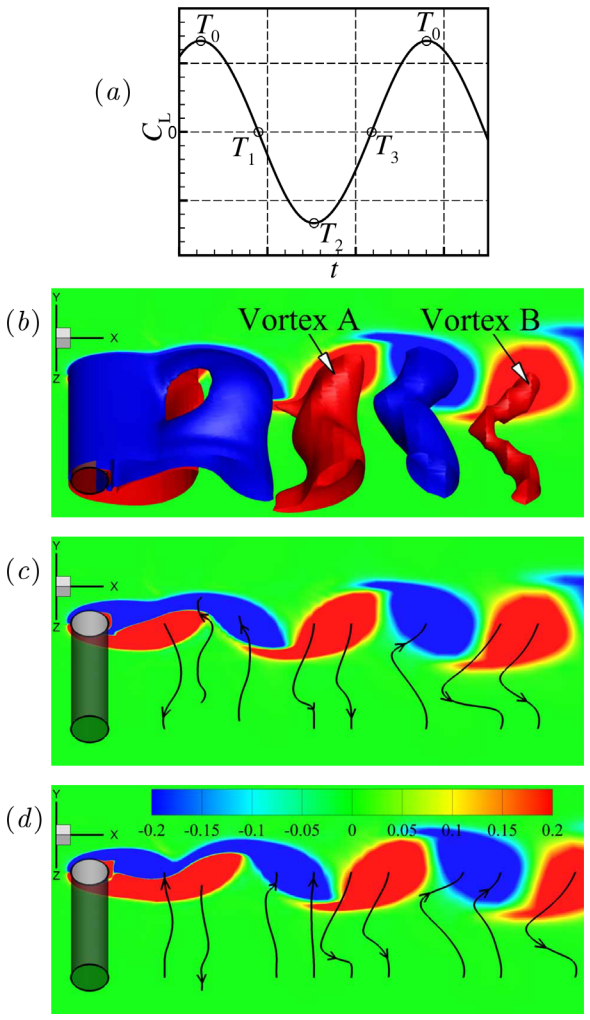

FIG. 5. (a) Schematic diagram of lift coefficient C_L along with time, where T_0, T_1, T_2, and T_3 are four typical times in a whole shedding period. (b) Isosurfaces of dimensionless spanwise vorticity $\omega_z = \pm 0.5$ (red/blue) in the near wake at $t = T_0$, typical vortex lines at (c) $t = T_0$ and (d) $t = T_1$ in shedding primary vortices at $Re = 195$ and nondimensional axial cylinder length L_Z of 4 through DNS,[4] where the background at $z = 0$ is illustrated by contours of ω_z with legend in figure (d), and the cylinder is denoted by the gray translucent surface. The incoming flow is from left to right.

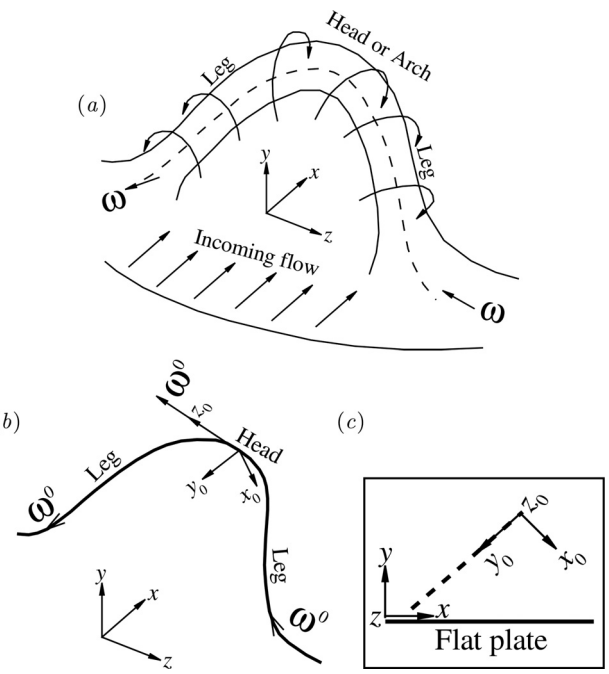

FIG. 6. (a) Sketch of Theodorsen's hairpin vortex paradigm.[6] Simplified schematic diagrams of Theodorsen's hairpin vortex as a vortex line located in the center of hairpin vortex from (b) the top view and (c) the side view, where local system $(x_0, y_0,$ and $z_0)$ locates at the head, and dashed line in figure (c) denotes the vortex line slanted downstream.

flow domain can be used in this local vortex line. This result indicates that such a hairpin vortex maintains its curved formation at the next time, before the vorticity totally vanishes.

In summary, whether solid walls are introduced or not, under present circumstances (i.e., without any kind of disturbance), the already curved vortex line at $t = t_0$ is still curved at $t = t_1$ with the existence of local vortex stretching and twisting effects, mainly due to inertial forces, before its vorticity completely dissipates.

C. Third case: Straight vortex lines at $t = t_0$ with introduced disturbances

Some conditions in the present analysis are prescribed as follows.

First, it should be stated that in the present subsection, the inviscid fluid is not taken into account. The physical reason is mainly attributed to the free-slip boundary condition of the introduced disturbed velocity or vorticity. For example, in the circle region of $x^2 + y^2 = r^2 \le 1$, the nonzero disturbed spanwise velocity w^0 along the z-axis is introduced into the original 2D velocity field (u^0, v^0) in the (x, y) plane at the initial time $t = t_0$, e.g., $w^0 = 1$ at $r \le 1$ and $w^0 = 0$ at $r > 1$. Because of the inviscid fluid and the resultant disappearance of shear stress at the radial boundary of such a circular region $r = 1$, there exists a discontinuous gradient, i.e., $\frac{\partial w^0}{\partial x} = \frac{\partial w^0}{\partial y} = 0$ if $r \neq 1$ but $\frac{\partial w^0}{\partial x} = \frac{\partial w^0}{\partial y} \to \infty$ when $r = 1$. Consequently, based on the definition of the vorticity vector, there is a singularity in the induced streamwise vorticity $\omega_x^0 = \frac{\partial w^0}{\partial y}$ and vertical vorticity $\omega_y^0 = -\frac{\partial w^0}{\partial x}$ at $r = 1$. A similar situation also occurs in the boundary of the introduced vortex with a certain size and vorticity when the viscosity and consequent viscous diffusion vanish. Once the fluid viscosity is introduced, such singularity trouble in vorticity distribution disappears. Hence, only viscous flow is analyzed and discussed in the following context.

Then, the finite flow domain with solid walls is the main concern here. The main reason is that twisted vortices in the flow region far from solid walls are diffused and dissipated due to the action of viscous forces, as well as disturbed vorticity temporarily introduced, from the above-stated analysis and Fig. 5(b) as an example.

Accordingly, the focus is mainly placed on the immediate neighborhood of solid walls. Here, three velocity components in the local velocity field are assumed to have the same magnitudes, i.e., $u \sim v \sim w$. Then, the magnitude of inertial forces is approximately $u^2/\Delta y$, where Δy is the normal height of the local flow region away from the solid surface, while the magnitude of viscous forces is approximately $u/(Re\Delta y^2)$. When viscous forces are far greater than inertial forces, then $\Delta y \ll (uRe)^{-1}$, i.e., in the immediate neighborhood of solid walls. When the height Δy exceeds $(uRe)^{-1}$, viscous forces are gradually weakened and inertial forces become dominant.

In the present subsection, two typical flows are also illustrated to present the process of 2D straight vortex lines twisted to be 3D curved vortex lines. One is the 3D wake transition of a straight circular cylinder. The other is a transition in the boundary layer.

Finally, natural disturbances are mainly considered and discussed here, such as perturbations due to 3D instability or turbulence. However, for artificial disturbances, such as geometric disturbances introduced in square section cylinders[29] and circular section cylinders[30] at $Re = 100$, the original 2D wake flow becomes 3D wake flow, similar to the appearance of pure mode A,[4] as shown in Fig. 5(b), or even the complete suppression of Kármán vortices.

Consequently, analytical results in the previous work[23] can be applied here. Under the condition of $\Delta y \ll (uRe)^{-1}$, only viscous forces in the vorticity equation, Eq. (3), are applied first, i.e., $\nabla^2\boldsymbol{\omega} = 0$. At the initial time t_0, there is no disturbance in original 2D shear flows with $(\boldsymbol{\omega}^0 \cdot \nabla)\boldsymbol{u}^0 = 0$. After a kind of disturbance is introduced at the next time t_1, 3D vorticity field then appears although the theoretical analysis is carried out in the steady flow.[23] Once this 3D vorticity field $\boldsymbol{\omega}^1$ is generated, there are $\boldsymbol{\omega}_\parallel^1 \neq \boldsymbol{\omega}^0$ and $\boldsymbol{\omega}_\perp^1 \neq 0$. In the meantime, although inertial forces are neglected in this flow region $\Delta y \ll (uRe)^{-1}$, they still exist but are physically small. This 3D vorticity field $\boldsymbol{\omega}^1$ obtained by only viscous forces leads to nonzero vortex stretching and twisting appearing, i.e., $(\boldsymbol{\omega}^1 \cdot \nabla)\boldsymbol{u}^1 \neq 0$ in the disturbed flow region $\Delta y > 0$. It further results in $\boldsymbol{\omega}_\parallel^1 \neq \boldsymbol{\omega}^0$ and $\boldsymbol{\omega}_\perp^1 \neq 0$. It should be mentioned here that, in this work,[23] when the vertical distance Δy becomes zero at solid walls, the theoretical vorticity distribution clearly illustrates $\boldsymbol{\omega}_\parallel^1 \neq \boldsymbol{\omega}^0$ and $\boldsymbol{\omega}_\perp^1 \neq 0$, while $(\boldsymbol{\omega}^1 \cdot \nabla)\boldsymbol{u}^1 = 0$ and $(\boldsymbol{u}^1 \cdot \nabla)\boldsymbol{\omega}^1 = 0$. This means that the original 2D vortex line at solid walls is stretched and twisted by only viscous forces with 3D disturbances, while inertial forces always disappear at solid walls and, thus, have no physical effect on the vortex stretching and twisting. This is a key feature in that the origin of vortex stretching and twisting is determined by viscous forces rather than inertial forces. As time passes and the vertical distance Δy increases, vortex stretching and twisting due to inertial forces are gradually dominant.

1. 3D wake transition of a straight circular cylinder

Different from the previous Reynolds number range of $Re < 140$–145 in Sec. III A 2, the Reynolds number in the present analysis exceeds 140–145, in which 3D instability occurs first near cylinder surfaces.[5] With increasing Reynolds number, originally 2D or straight vortex lines near cylinder surfaces become 3D or curved vortex lines, remarkably indicated by the appearance or generation of streamwise and vertical components of vorticity, i.e., ω_x and ω_y. The initial stage of such a 3D vortex structure in a 2D boundary layer separation flow was first investigated by Yokoi and Kamemoto.[31,32] The wavy separation line on the surface of a circular cylinder is observed in the experiments, as shown in Fig. 7(a). Correspondingly, the laminar boundary layer is wavily separated from the side of a separated region. It is clearly shown in Fig. 7(a) that the originally parallel surface streamlines in the upstream region, illustrated by solid lines, become 3D after leaving the surface, and the distances between neighboring streamlines become either wider or narrower. This indicates that the spanwise velocity appears near such a wavy separation line, associated with skewed streamlines along the z-axis. Consequently, according to the definition of the vorticity vector, ω_x and ω_y are generated behind those wavy separated regions.

Moreover, in the Reynolds number range from 145 to 195, the initially generated stage of pure mode A gradually appears through DNS, as reported in recent work.[5] The main characteristics in the present stage are vortex lines in primary vortex cores still almost 2D or straight, as shown in Fig. 7(b) or 7(c) at $Re = 190$, compared with those in the fully developed stage in Fig. 5(c) or 5(d) at $Re = 195$. Another prominent feature, different from the flow at $Re < 140$, is the initial generation of streamwise and vertical components of vorticity on the cylinder surface, typically as shown in Figs. 7(d) and 7(e).

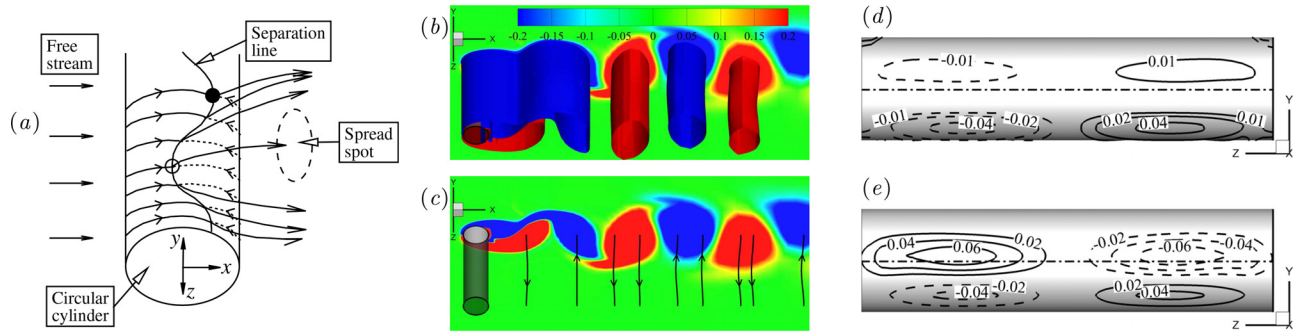

FIG. 7. (a) Schematic diagram of the 3D separation from a circular cylinder,[31,32] where symbols ○ and ● denote upstream and downstream singular separation points with zero shear stress at walls, respectively. In the near wake of a circular cylinder at $t = T_0$, $Re = 190$ and dimensionless axial cylinder length $L_Z = 4$ through DNS,[5] (b) isosurfaces of nondimensional spanwise vorticity $\omega_z = \pm 0.5$ (red/blue), (c) typical vortex lines in primary vortex cores and contours of dimensionless additional vorticities, (d) ω_x (with ± 0.01, ± 0.02, and ± 0.04), and (e) ω_y (with ± 0.02, ± 0.04, and ± 0.06), on the rear surface of cylinder. Note that in figures (b) and (c), the cylinder is denoted by the gray translucent surface, the free stream is from left to right, and the background at $z = 0$ is demonstrated by contours of ω_z. And in figures (d) and (e), the dash dot line denotes the wake center plane of $y = 0$, and solid and dashed lines denote positive and negative values of additional vorticities, respectively.

These results agree well with the above statements in Yokoi and Kamemoto.[31,32]

Therefore, both experimental observations and DNS confirm that the original 2D or straight vortex lines become 3D or curved vortex lines first near cylinder surfaces due to 3D instability associated with the generation of streamwise and vertical vorticities.

2. Transition from 2D steady flow to 3D vortex structures in the boundary layer

Generally, the experimental results demonstrating the appearance of hairpin vortices are shown in the basic sketch in Fig. 8. The transition in the laminar boundary layer is initially governed by stable laminar flow, the instability of traveling, 2D T–S waves, primary stability theory, and the appearance of unsteady, laminar, and 3D waves

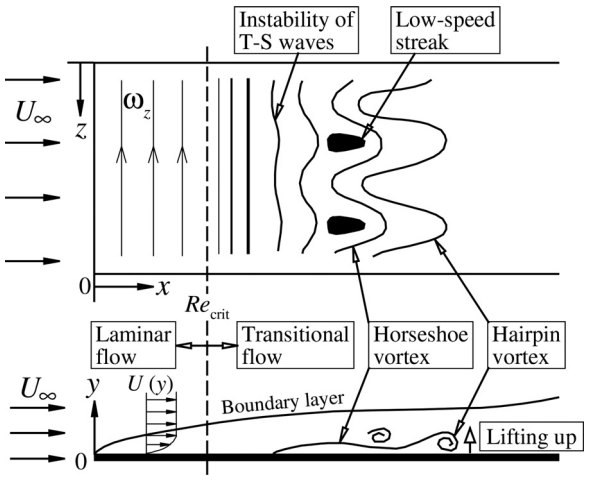

FIG. 8. Schematic diagram of the formation of T–S waves and horseshoe and hairpin vortices in the transition of the laminar boundary layer of a flat plate at zero incidence,[24,33] where Re_{crit} is the critical Reynolds number with the occurrence of transition.

due to secondary instabilities and a characteristic Λ-structure vortex formation,[24,33] as shown in Fig. 8. The 3D disturbance with increasing T–S instability waves leads to the formation of streamwise vortex pairs in the viscous sublayer.[34] This periodic distribution of streamwise vortex pairs along the span further results in the redistribution of the streamwise velocity along the span, forming staggered streaks with high and low speeds in the buffer region.[35] The streaks and the vortices are involved in a self-sustaining nonlinear cycle.[36,37] Moreover, the signal of velocity fluctuations is characterized by so-called spikes, which denote the appearance of local high shearing regions together with the point of inflection velocity profiles. With increasing disturbance, streamwise vortex pairs around low-speed streaks develop into a horseshoe vortex.[38] The horseshoe vortex can be lifted up under the vortex-induced vortex mechanism owing to viscous forces through theoretical analysis[7] and, thus, becomes a hairpin vortex.

Accordingly, both experiments and theoretical analysis clearly illuminate that 3D disturbances lead to the original 2D vortex lines in stable laminar flow being 3D with the appearance of a lifting-up hairpin vortex, also accompanied by the generation of streamwise and vertical components of vorticity, as shown in Fig. 6(b).

In summary, through analysis in flows past a straight bluff body or a flat plate at zero incidence, it is clarified that 3D natural disturbances are one of the key conditions in the transition from the 2D flow state to the 3D flow state as well as the transition from straight vortex lines to curved vortex lines. Based on the indirect physical mechanism of viscous forces in vortex stretching and twisting,[23] these phenomena are closely related to solid walls, 3D disturbances, and fluid viscosity.

IV. CONCLUSIONS

In this paper, the physical origin of vortex stretching and twisting is theoretically investigated and discussed in detail. In the present fluid dynamic system, such as incompressibility of the fluid and conservative body forces, only inertial and viscous forces are considered and analyzed as generation or enhancement mechanisms in vortex stretching and twisting. Two key conditions, namely, solid walls and 3D disturbances, are introduced, as reported in the previous work.[23] Three different cases are analyzed according to whether 3D disturbances are introduced. Moreover, the analysis in two typical flows, namely, the

near wake of a bluff body and the boundary layer at a flat plate, is also carried out, as in typical cases with the introduction of solid walls.

The first case is the straight vortex line at the initial time without any kind of disturbance. Through theoretical analysis and experimental observation, whether solid walls are introduced or not, the straight vortex line at the initial time is still straight at the next time with the absence of any vortex stretching and twisting.

The second case is the curved vortex line at the initial time without any kind of disturbance. According to theoretical analysis, experiments, and numerical simulations, it is confirmed that whether solid walls are introduced or not, the already curved vortex line at the initial time is still curved at the next time with the existence of local vortex stretching and twisting effects, mainly due to inertial forces, before the vorticity totally dissipates due to the action of fluid viscosity.

The key analysis is the third case with the straight vortex line at the initial time under 3D natural disturbances, coupled effects of solid walls, and viscous forces. The 3D wake transition of a straight circular cylinder is analyzed through experimental observations and direct numerical simulations, and the transition of the laminar boundary layer at a flat plate is also presented by experiments and theoretical analysis. It is verified that 3D natural disturbances are one of the key conditions in the transition from straight vortex lines to curved vortex lines. By means of the indirect physical mechanism of viscous forces in vortex stretching and twisting,[23] these 3D transitional phenomena are closely related to solid walls, 3D (natural or artificial) disturbances, and fluid viscosity. Particularly, at solid walls, the vortex stretching and twisting still can be generated by viscous forces with 3D disturbances, but inertial forces totally disappear.

Consequently, according to the above analysis of 3D transitional phenomena mainly appearing in the immediate neighborhood of solid walls, where viscous forces are greater than inertial forces, it is clarified that viscous forces coupled with two key conditions are the generation mechanism of vortex stretching and twisting, while inertial forces independent of two key conditions are the enhancement mechanism once the vortex stretching and twisting already appear.

AUTHOR DECLARATIONS

Conflict of Interest

The authors have no conflicts to disclose.

Author Contributions

Liming Lin: Conceptualization (lead), Formal analysis (lead), Investigation (lead), and Writing – original draft (lead). **Yingxiang Wu:** Conceptualization (supporting) and Formal analysis (supporting).

DATA AVAILABILITY

The data that support the findings of this study are available from the corresponding author upon reasonable request.

REFERENCES

[1]C. H. K. Williamson, "Vortex dynamics in the cylinder wake," Annu. Rev. Fluid Mech. **28**, 477–539 (1996).
[2]R. D. Henderson, "Nonlinear dynamics and pattern formation in turbulent wake transition," J. Fluid Mech. **352**, 65–112 (1997).
[3]H. Jiang, L. Cheng, S. Draper, H. An, and F. Tong, "Three-dimensional direct numerical simulation of wake transitions of a circular cylinder," J. Fluid Mech. **801**, 353–391 (2016).
[4]L. M. Lin and Z. R. Tan, "DNS in evolution of vorticity and sign relationship in wake transition of a circular cylinder: (Pure) mode A," Acta Mech. Sin. **35**, 1131–1149 (2019).
[5]L. M. Lin, "Initially generated pure mode A in the three-dimensional wake transition of a circular cylinder," Fluid Dyn. Res. **54**, 035504 (2022).
[6]T. Theodorsen, "Mechanism of turbulence," in *Second International Midwest Conference on Fluid Mechanics* (Ohio State University, 1952), pp. 1–19.
[7]L. M. Lin and Y. X. Wu, "Theoretical analysis of vorticity in a hairpin vortex in the viscous sublayer of a laminar boundary layer," Eur. J. Mech.-B/Fluids **94**, 106–120 (2022).
[8]T. Dombre, U. Frisch, J. M. Greene, M. Hénon, A. Mehr, and A. M. Soward, "Chaotic streamlines in the ABC flows," J. Fluid Mech. **167**, 353–391 (1986).
[9]V. N. Golubkin and G. B. Sizykh, "Some general properties of plane-parallel viscous flows," Fluid Dyn. **22**, 479–481 (1987).
[10]S. Changchun and H. Yongnian, "Some properties of three-dimensional Beltrami flows," Acta Mech. Sin. **7**, 289–294 (1991).
[11]V. Trkal, "A note on the hydrodynamics of viscous fluids (translated by I. Gregora)," Czech. J. Phys. **44**, 97–106 (1994).
[12]O. I. Bogoyavlenskij, "Infinite families of exact periodic solutions to the Navier-Stokes equations," Moscow Math. J. **3**, 263–272 (2003).
[13]O. Bogoyavlenskij and B. Fuchssteiner, "Exact NSE solutions with crystallographic symmetries and no transfer of energy through the spectrum," J. Geom. Phys. **54**, 324–338 (2005).
[14]H. K. Moffat, "Helicity and singular structures in fluid," Proc. Natl. Acad. Sci. U. S. A. **111**, 3663–3670 (2014).
[15]S. V. Ershkov, "Non-stationary helical flows for incompressible 3D Navier-Stokes equations," Appl. Math. Comput. **274**, 611–614 (2016).
[16]S. V. Ershkov, "About existence of stationary points for the Arnold-Beltrami-Childress (ABC) flow," Appl. Math. Comput. **276**, 379–383 (2016).
[17]D. Dierkes, A. Cheviakov, and M. Oberlack, "New similarity reductions and exact solutions for helically symmetric viscous flows," Phys. Fluids **32**, 053604 (2020).
[18]S. V. Ershkov, A. R. Giniyatullin, and R. V. Shamin, "On a new type of non-stationary helical flows for incompressible 3D Navier-Stokes equations," J. King Saud Univ.-Sci. **32**, 459–467 (2020).
[19]D. Küchemann, "Report on the IUTAM Symposium on concentrated vortex motion in fluids," J. Fluid Mech. **21**, 1–20 (1965).
[20]H. K. Moffatt, S. Kida, and K. Ohkitani, "Stretched vortices—The sinews of turbulence; large-Reynolds-number asymptotics," J. Fluid Mech. **259**, 241–264 (1994).
[21]J. Z. Wu, H. Y. Ma, and M. D. Zhou, *Vorticity and Vortex Dynamics* (Springer, Berlin/Heidelberg/New York, 2006).
[22]S. I. Green, *Fluid Vortices* (Kluwer Academic Publishers, Norwell, 1995).
[23]L. M. Lin and Y. X. Wu, "Indirect physical mechanism of viscous forces: Vortex stretching and twisting," Phys. Fluids **34**, 073101 (2022).
[24]H. Schlichting, *Boundary Layer Theory*, 7th ed. (McGraw-Hall Book Company, 1979).
[25]L. P. Bernal and A. Roshko, "Streamwise vortex structure in plane mixing layer," J. Fluid Mech. **170**, 499–525 (1986).
[26]P. M. Gresho, "Incompressible fluid dynamics: Some fundamental formulation issues," Annu. Rev. Fluid Mech. **23**, 413–453 (1991).
[27]C. B. Lee and X. Y. Jiang, "Flow structures in transitional and turbulent boundary layers," Phys. Fluids **31**, 111301 (2019).
[28]A. A. Townsend, "Equilibrium layers and wall turbulence," J. Fluid Mech. **11**, 97–120 (1961).
[29]R. M. Darekar and S. J. Sherwin, "Flow past a square-section cylinder with a wavy stagnation face," J. Fluid Mech. **426**, 263–295 (2001).
[30]L. M. Lin, X. F. Zhong, and Y. X. Wu, "Flow around a circular cylinder with radial disturbances at a low Reynolds number," in paper Presented at the Twenty-Third International Offshore and Polar Engineering, Anchorage, Alaska, June 30-July 5, 2013.
[31]Y. Yokoi and K. Kamemoto, "Initial stage of a three-dimensional vortex structure existing in a two-dimensional boundary layer separation flow (observation of laminar boundary layer separation over a circular cylinder by flow visualization)," JSME Int. J., Ser. II **35**, 189–195 (1992).
[32]Y. Yokoi and K. Kamemoto, "Initial stage of a three-dimensional vortex structure existing in a two-dimensional boundary layer separation flow (visual

observation of laminar boundary layer separation over a circular cylinder from the side of a separated region)," JSME Int. J., Ser. B **36**, 201–206 (1993).
[33]F. M. White, *Viscous Fluid Flow* (McGraw Hill, New York, 1974).
[34]M. R. Head and P. Bandyopadhyay, "New aspects of turbulent boundary layer structure," J. Fluid Mech. **107**, 297–338 (1981).
[35]S. J. Kline, W. D. Reynolds, F. A. Schraub, and P. W. Runstadler, "The structure of turbulent boundary layers," J. Fluid Mech. **30**, 741–773 (1967).
[36]J. Jiménez, G. Kawahara, M. P. Simens, M. Nagata, and M. Shiba, "Characterization of near-wall turbulence in terms of equilibrium and bursting solutions," Phys. Fluids **17**, 015105 (2005).
[37]W. Schoppa and F. Hussain, "Coherent structure generation in near-wall turbulence," J. Fluid Mech. **453**, 57–108 (2002).
[38]D. Swearingen and R. F. Blackwelder, "The growth and breakdown of streamwise vortices in the presence of a wall," J. Fluid Mech. **182**, 255–290 (1987).